Spectrochimica Acta Part B: Atomic Spectroscopy 216 (2024) 106946

Contents lists available at ScienceDirect

Spectrochimica Acta Part B: Atomic Spectroscopy

journal homepage: www.elsevier.com/locate/sab

New energy levels of atomic holmium discovered by laser spectroscopy in the near infrared spectral range

Seda Kın Barka [a,b], Günay Başar [c], Sophie Kröger [d,*], Gönül Başar [e]

[a] Istanbul Technical University, Graduate School, Physics Engineering Program, Maslak TR-34469, Istanbul, Türkiye
[b] Acibadem Mehmet Ali Aydinlar University, Vocational School of Health Services, Opticianry Program, Atasehir TR-34752, Istanbul, Türkiye
[c] Istanbul Technical University, Faculty of Science and Letters, Physics Engineering Department, Maslak TR-34469, Istanbul, Türkiye
[d] Hochschule für Technik und Wirtschaft Berlin, Wilhelminenhofstr. 75A, Berlin D-12459, Germany
[e] Istanbul University, Faculty of Science, Physics Department, Vezneciler TR-34134, Istanbul, Türkiye

ARTICLE INFO

Keywords:
Atomic data
Laser spectroscopy
Fine structure
New energy levels

ABSTRACT

A combination of optogalvanic spectroscopy and laser-induced fluorescence spectroscopy with a continuous wave tunable single mode Ti-Sa laser was applied to find new energy levels of atomic holmium. Free and excited holmium atoms were produced in a liquid nitrogen-cooled hollow-cathode lamp. In this study, we examined 35 spectral lines of Ho I in the near-infrared wavelength range from 698 nm to 833 nm. Altogether, 16 new energy levels have been discovered, 5 levels of even parity and 11 levels of odd parity. Another four energy levels have been discovered but have already been published by another research group. Data on the hyperfine structure for the new levels are presented. Additionally, hyperfine structure data of three known levels of even parity were determined for the first time. The existence of the new energy levels was confirmed by analyzing 60 lines of previously measured Fourier transform spectra to precisely determine the energy of the levels.

1. Introduction

There is a great need for experimental data on the structure of complex atoms. Atoms with more than one open valence electron shell in an excited state, particularly transition metals, are referred to as complex atoms. The complexity increases with the angular momentum quantum number of the valence electrons. Atoms with open f electron shells, i.e. lanthanides and actinides, show the greatest complexity. Data on the structure of complex atoms are of great interest for applications in astrophysics and other areas of physics. The amount and accuracy of the experimental data play a key role in the future optimization of the theoretical description both in ab initio calculations and semi-empirical analyses of atomic structures.

Holmium (Ho), with $Z = 67$, is one of the atoms that belong to the lanthanide series. It has only one stable isotope, with an atomic mass number of $A = 165$ and a nuclear spin of $I = 7/2$. The neutral Ho atom (Ho I) has a ground state configuration of $[Xe]4f^{11}\,6s^2$. Ho has relatively high multipole moments, $\mu = 4.17\,(3)\,\mu_N$ and $Q = 2.7 - 3.6$ barn [1]. Ho is therefore considered to be among the strong candidates to be studied in various fields of physics, for discovering new energy levels and analyzing hyperfine structures.

Many studies have contributed to the formation of the atomic database of Ho I. The Ho I energy levels that were already known from [2–4] are summarized in the NIST Atomic Spectra Database [5]. Several publications have been released recently, including [6–8]. In the last six years alone, seven additional publications have been published that report on the discovery and research of new energy levels in Ho I [9–14]. Despite being a topic of research in various experimental and theoretical investigations in the last decades, there are still many gaps in knowledge about the atomic energy levels of Ho I. The focus of this study is to discover new energy levels and determine their corresponding magnetic dipole and electric quadrupole hyperfine structure constants A and B.

This paper presents the results of research carried out over the last four years. Originally, we discovered 20 new levels. In the meantime, four of them have also been discovered by another research group, bringing the total to 16 levels, which are published here for the first time.

2. Experiment

The measurements were carried out in the laser spectroscopy laboratory at Istanbul University. The experimental setup was the same as

* Corresponding author.
E-mail address: sophie.kroeger@htw-berlin.de (S. Kröger).

https://doi.org/10.1016/j.sab.2024.106946
Received 10 March 2024; Received in revised form 13 May 2024; Accepted 14 May 2024
Available online 17 May 2024

previous studies on other elements for the search of new levels [15,16].

A lab-made see-through hollow cathode lamp was used to produce free and excited Ho atoms [17]. The cathode consists of a hollow copper cylinder with an inner diameter of 3 mm, lined with a 0.125 mm thin Ho foil. The purity of the Ho foil is 99.9%. As buffer gas Neon was used with a pressure of about 1 mbar. The hollow cathode lamp ran with a discharge current of 60 mA. To reduce Doppler line broadening the cathode was cooled with liquid nitrogen.

A continuous wave tunable single mode Ti-Sa laser (Coherent MBR 110 with a maximum output power of 4 W) was used for the laser spectroscopic investigations. The maximal scan width was 20 to 35 GHz, depending on the wavelength range. The output power of the laser was reduced to about 1 W to reduce saturation broadening. The laser power remains almost constant throughout the entire scan. The absolute wavelength of the laser light was measured with the help of a commercial wavemeter (High Finesse 6–200, absolute accuracy 200 MHz). A temperature-controlled confocal Fabry-Perot interferometer with a free spectral range of FSR = 299.001 (8) MHz was used to calibrate the frequency scale of the measured spectra.

Optogalvanic spectroscopy (OGS) as well as laser induced fluorescence (LIF) spectroscopy could be applied simultaneosly. For both methods, the laser beam was intensity modulated by a mechanical chopper wheel with a modulation frequency of about 1 kHz and passed through the hollow cathode. For optogalvanic detection, the change of discharge current, caused by resonant absorption of laser light, was measured as a voltage change at a ballast resistor using a lock-in amplifier synchronized with the chopper wheel. Simultaneously, for LIF detection, the change of the fluorescence light caused by resonant absorption of laser light was measured with a photomultiplier tube (Hamamatsu R928). To select the fluorescence channel for LIF measurements, the fluorescence light is passed through a grating monochromator (McPherson 607 with 607 mm focal length and 1200 lines/mm). The wavelength of the monochromator could be determined with an uncertainty of about 0.2 nm. The signal from the photomultiplier was processed again using a lock-in amplifier. The resolution of the monochromator depends on the width of its slit, which can be adjusted. In our experiments, we chose a wider slit to obtain a stronger LIF signal. The resolution of the monochromator spectrum was not critical for our investigation, as we were able to identify the relevant fluorescence lines even with a larger slit width.

This setup allows for scanning either the laser wavelength while keeping the monochromator wavelength fixed or scanning the monochromator wavelength while keeping the laser at a fixed wavelength. Both options were alternately used for the targeted search for new levels, as described in Section 4. When scanning the monochromator, fluorescence lines can be observed and measured in positive and negative phases. A positive phase indicates a fluorescence transition from the upper level of the laser transition, while a negative phase indicates a fluorescence transition from the lower level of the laser transition.

During the monochromator scan, in addition to measuring the fluorescence signal using the lock-in amplifier, the emission light of the hollow cathode lamp is also measured without the lock-in amplifier. This simultaneous measurement helps in better identifying the fluorescence lines, as demonstrated in the case described below.

In addition to the laser measurements, we had access to FT spectra measured by some of the authors (GöB, SK) covering the wavelength range from 320 nm to 1750 nm. The spectra have already been used as the basis for several publications dealing with line classifications in different wavelength ranges [18–22] and with the investigation of the hyperfine structure [23]. The spectral accuracy of these calibrated spectra is better than 0.005 cm^{-1} across the entire wavelength range (see [18–22]).

Fig. 1 compares the optogalvanic spectrum with the FT spectrum in the same wavenumber range. Assuming that measurements were taken under similar discharge conditions of the hollow cathode, it is important to note three significant differences in the measurement methods:

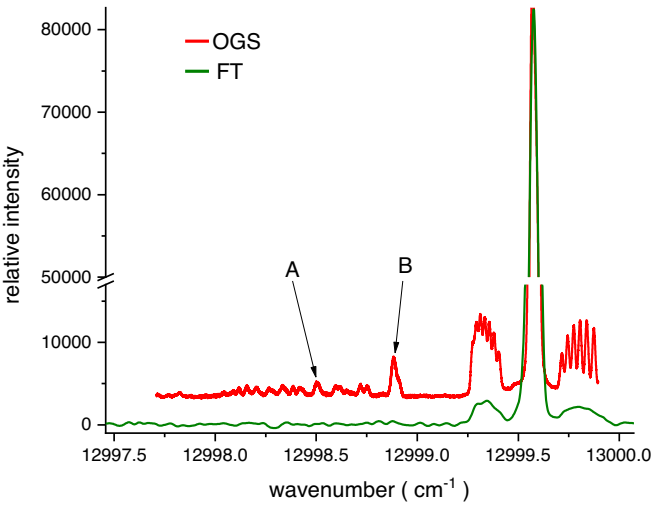

Fig. 1. Comparison of the laser spectroscopic optogalvanic measurement and the FT spectrum. Both spectra have been normalized to ensure that the strongest peaks have the same height in both spectra. To make the small peaks more visible, there is a scaling break on the y-axis. The arrows labeled 'A' and'B' indicate the positions where the laser wavelength was fixed for the subsequent monochromator scans (please refer to Section 4 for more information).

- The optogalvanic measurement is generally more sensitive than the FT spectroscopy.
- The optogalvanic measurement provides better spectral resolution compared to FT spectroscopy. This is evident in the strong line with the 'butterfly' structure at the right edge, where the small components in the optogalvanic spectrum are resolved, but unresolved in the FT spectrum.
- Due to the saturation effect, the weak hfs components appear in the optogalvanic spectrum with increased intensity compared to the strong hfs component – whereas in the FT spectrum, the intensities correspond exactly to the theoretical intensity. This can also be clearly recognized by the strong line with the 'butterfly structure' on the right-hand edge: The intensities are normalized in both spectra in such a way that the maximum of the line is equally high in both cases; the small hfs components appear significantly higher in the optogalvanic spectrum. This effect has both advantages and disadvantages.

3. Hyperfine structure analysis

When analyzing spectral lines of Ho, the hyperfine structure (hfs) serves as an important fingerprint of the two levels involved in the transition. This section explains the analysis of the hfs of the spectral lines before the search for new levels is presented in the next section. Examples of beautiful hfs fingerprints are shown in Fig. 2.

For three lines, the width of the hfs surpasses the scanning width of the laser of 20 to 35 GHz. In these cases, the spectrum was recorded in two segments with overlapping areas. An example is shown in Fig. 2e.

To derive the hfs constants A and B of the upper and lower energy levels involved in the laser transition from the recorded LIF spectra, the computer program Fitter [24] was used. The program fits a parameterized model of the hfs with least squares optimization to the experimental spectrum. The list of parameters comprises.

- the center of gravity of the total hfs,
- the magnetic dipole hfs constant A and the electric quadrupole hfs constant B of the upper and of the lower level,
- two parameters to describe the height and slope of the background,
- the intensity for each individual hfs component, and,

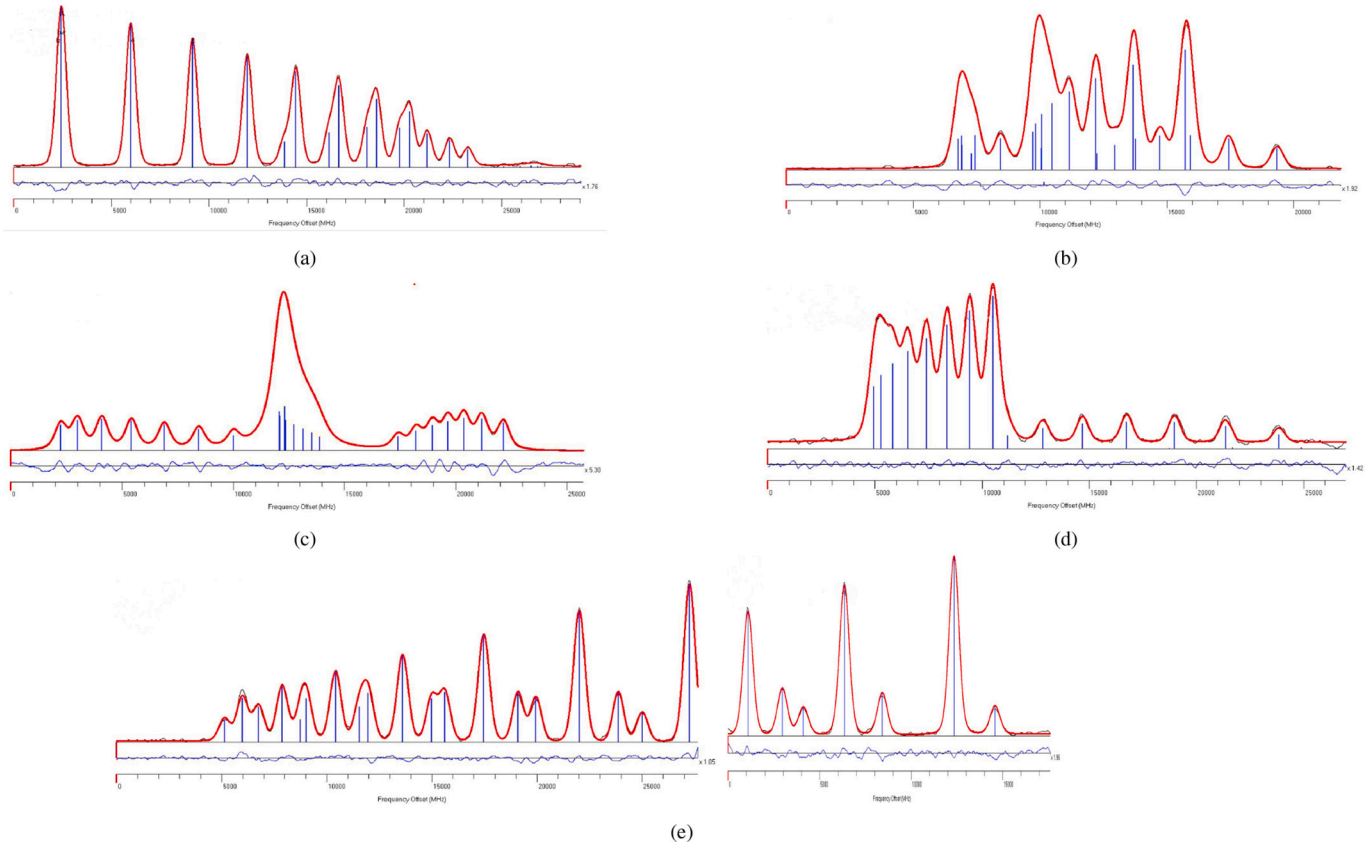

Fig. 2. Beautiful examples for fingerprints of hyperfine structure (see text for explanations); Combined experimental spectra and best-fitted curve of hfs; in the lower part of the plots, the residuals between the experiment and the fit are given; the components are marked by vertical blue bars. (For interpretation of the references to colour in this figure legend, the reader is referred to the web version of this article.)
(a) line at $\lambda = 832.836$ nm or $\sigma = 12003.87$ cm^{-1}, transition from 27,649.51 cm^{-1}, $J = 15/2$ to 39,653.44 cm^{-1}, $J = 13/2$.
(b) line at $\lambda = 762.757$ nm or $\sigma = 13106.73$ cm^{-1}, transition from 18,858.19 cm^{-1}, $J = 13/2$ to 31,964.93 cm^{-1}, $J = 13/2$.
(c) line at $\lambda = 771.151$ nm or $\sigma = 12964.07$ cm^{-1}, transition from 27,113.28 cm^{-1}, $J = 11/2$ to 40,077.35 cm^{-1}, $J = 11/2$.
(d) line at $\lambda = 750.129$ nm or $\sigma = 13327.37$ cm^{-1}, transition from 29,443.09 cm^{-1}, $J = 17/2$ to 42,770.41 cm^{-1}, $J = 15/2$.
(e) line at $\lambda = 722.232$ nm or $\sigma = 13842.15$ cm^{-1}, transition from 18,821.25 cm^{-1}, $J = 11/2$ to 32,663.47 cm^{-1}, $J = 11/2$; example of a line whose splitting exceeds the scanning range of the laser and was recorded in two parts with four overlapping hfs components, measured in the left and right parts.

- depending on the choice of profile function, profile parameters for each individual hfs component.

For our investigation, a Voigt function was chosen as the profile function, which requires two parameters to define, the full widths of half maximum (FWHM) of its Gaussian and the Lorentzian parts. For all parameters, it can be specified whether they should be free, linked to other parameters, or kept constant at a predefined value. For the intensity parameters, there is the option to couple them according to the theoretical intensity ratios for hyperfine structure components or to couple them with any ratio.

As a result of the high laser power, most measured lines show a significant reduction in the intensity of the strong hfs components due to saturation effects. This leads to an apparent intensity increase of the weak components. In this case, the theoretical intensity ratios are not applicable, thus the intensities of the individual components were set free. If this was not applicable, due to overlapping components or very high noise level, the intensities of individual components were coupled considering the saturation effect. For this purpose, a saturation parameter I_{sat} introduced in [27,28] was implemented, which specifies the relative intensity increase depending on the quantum number. The hfs simulation program HFSSIM [29] was used to determine the appropriate I_{sat} parameter by comparing the experimental spectrum with a corresponding simulation. The HFSSIM program then calculated the intensity ratios based on the determined I_{sat} value. These intensity ratios were then determined during the fitting process using the FITTER program.

tw: this work.

In the case of well-resolved strong lines – as we know from previous laser spectroscopy studies - the FWHM of the hyperfine structure components is also influenced by saturation. This mainly concerns the Lorentzian contribution. The FWHM of the Lorentzian contribution of the individual hfs components varies due to the broadening. The Gaussian FWHM, on the other hand, remains relatively unaffected by the saturation effect. To account for the broadening caused by saturation effects, we chose the same Gaussian FWHM value for all well-resolved lines for all hfs components within a line. We then coupled the Lorentz width parameters for each group of hfs components with the same ΔF to the total angular momentum of the lower and upper hfs levels.

For some poorly resolved and/or noisy lines, the number of fitting parameters had to be further reduced to obtain reliable results. In these cases, the values of the hfs constants A and B of the lower level were fixed to values from the literature, if available, or in one case, to values derived from other lines measured in the present work. A list of the hfs constants that had been fixed during the fit is given in Table 1. The lines in which hfs constants have been fixed are marked in the relevant data tables.

Table 1
Experimental hyperfine structure constants A and B which have been fixed during the fit.

E (cm^{-1})	J	p	A (MHz)	B (MHz)	ref.
17,059.35	13/2	e	556.1 (0.7)	−1217 (40)	[25]
18,651.53	15/2	e	863.40 (0.16)	−2740 (16)	[11]
23,861.17	9/2	e	279 (4.5)	−39 (300)	[2]
23,946.16	11/2	e	618.5 (0.5)	−2265 (18)	[11]
23,955.68	13/2	e	951.93 (0.21)	−2451 (15)	[11]
24,014.22	13/2	e	901.28 (0.21)	−1404 (13)	[11]
24,357.92	15/2	o	840 (3)	−1874 (150)	[2]
24,660.80	15/2	e	752.5 (0.3)	−2469 (29)	[11]
24,740.52	13/2	e	707.8 (1.1)	−771 (46)	[26]
26,957.70	15/2	e	1514.8 (0.5)	510 (40)	[23]
27,556.90	9/2	e	1121.1 (0.5)	847 (7)	[6]
27,640.21	11/2	o	1515.2 (0.5)	−645 (7)	[6]
29,443.09	17/2	o	1061 (3)	2084 (150)	[2]
29,531.25	17/2	o	1218.2 (3.0)	122 (182)	[10]
29,692.67	19/2	o	529 (3)	2143 (150)	[2]
29,834.05	15/2	o	1050.4 (1.9)	36 (103)	[25]
40,077.35	11/2	o	1143.8 (0.5)	−635 (10)	tw

Notes: Values from [2] are converted from 10^{-3} cm^{-1} to MHz.

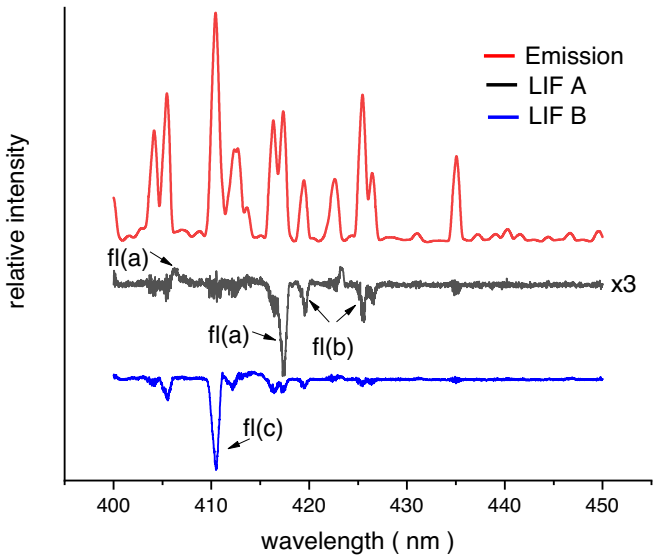

Fig. 3. Section of the monochromator scan for the range from 400 to 450 nm. The emission spectrum of the hollow cathode is shown at the top (in red). Below are two different measurements of the LIF signal at different laser wavelengths 'A' and'B' according to the values marked by arrows in Fig. 1. The measurement labeled 'A' has a weaker signal. To see it clearly in the comparison, the measurement data was multiplied by a factor of 3. The positions labeled with fl(a), fl(b), and fl(c) indicate the wavelengths of fluorescence used for the subsequent LIF measurements. If a letter refers to two different wavelengths with two arrows, it means that the same structure was detected with both wavelengths. If necessary, a phase offset of 180° was applied in the lock-in for positive LIF signal. (For interpretation of the references to colour in this figure legend, the reader is referred to the web version of this article.)

4. Search for new levels

The discovery of new energy levels in the present work was based on unclassified and unclassifiable lines in the Ho spectrum. Unclassifiable means that there are no known energy levels that can be used to explain a transition. The unclassified lines originate from three different sources:

- unclassified lines observed in FT spectra,
- using random optogalvanic laser scans for the search of unclassified lines, and
- lines observed by chance as extra peaks within an optogalvanic spectrum of a spectral line of previous measurements that do not belong to the line under investigation in this work.

At the beginning of each examination of an unclassified line, the wavelength of the laser was set to the wavelength of the unclassified line, and an optogalvanic spectrum covering the scan width of the laser was measured. For example, Fig. 1 shows multiple OGS spectra taken consecutively over 2 cm^{-1}. In the figure, some unclassified lines belong to the third category. These lines are the ones observed by chance as extra peaks in an optogalvanic spectrum. Adjacent to a strong line with a center of gravity at 12999.58 cm^{-1}, an optogalvanic signal was detected at the left edge of the spectrum, which could not be classified. This signal ultimately led to the discovery of two new levels. In the FT spectrum, there is no signal observed that exceeds the noise level at this point.

The next step was to adjust the laser wavelength to the most intense peak of the optogalvanic spectrum. First, the monochromator scan was performed with the fixed laser wavelengths marked by the arrows labeled 'A' in Fig. 1. The monochromator was then scanned in the range of 400 nm to 650 nm in parts of 50 nm. As discussed in Section 2 the emission spectrum of the hollow cathode lamp is recorded in parallel to the LIF signal. A section of the corresponding monochromator spectrum for this example is shown in Fig. 3. The emission spectrum of the hollow cathode is shown at the top (in red). Below are two different measurements of the LIF signal at different laser wavelengths 'A' and'B' according to the values marked by arrows in Fig. 1. The measurement labeled 'A' has a weaker signal. To see it clearly in the comparison, the measurement data was multiplied by a factor of 3. The comparison with the emission spectrum (upper curve) helps to better assign the fluorescence peaks that can be seen in the LIF signal (lower curves). When the monochromator passes strong emission lines, the LIF signal shows an increase in noise. However, 'real' LIF signals can be clearly distinguished from this noise and recognized as peaks where a clear separation from the zero line can be seen.

Due to inelastic collisions in the plasma, the energy transferred by the laser to the plasma is also transferred to other levels that are not directly involved in the laser transition. This causes additional lines to appear in the monochromator spectra, which are not connected to the levels of the laser transition.

If LIF peaks were detected, the next step was to set the monochromator to one of these wavelengths and scan the laser again. All the different LIF peaks were tested (as 'fl(a)', 'fl(b)', and 'fl(c)' in Fig. 3).

The program Elements [30,31] was used to support the attempt to classify the fluorescence lines. This program is based on input data of all known fine structure and hyperfine structure data from Ho I and Ho II.

Occasionally, different structures were detected at different fluorescence wavelengths during the laser scan - as in this case. In Fig. 4 the resulting LIF laser scan spectra are shown for different fluorescence wavelengths. The letters on the LIF curves indicate the fluorescence wavelengths corresponding to the wavelength positions shown in Fig. 3. Here, the LIF spectra were compared to the previously displayed OGS spectrum in Fig. 1.

Two different hfs spectra were detected here, each leading to the discovery of a new level. The corresponding new upper levels are indicated in Fig. 4. In this particular case, these two hfs spectra (a and b in Fig. 4) were not enough to explain the entire structure observed in the OGS spectrum (red spectrum in Fig. 4), as further peaks can be seen in the OGS spectrum to the right of the two structures (a and b). Therefore, another monochromator scan was performed, this time with the laser wavelength marked as'B′ in Fig. 1. The corresponding measurement of the monochromator scan can be seen in the lowest curve in Fig. 3. The lowest curve in Fig. 4 belongs to the negative peak in the monochromator scan ('fl(c)' in Fig. 3). Note, if a peak with a negative phase was detected in the monochromator scan, the phase was rotated 180° at the lock-in amplifier for the laser scan to measure the hfs spectrum as a positive LIF signal (which is easier for further data evaluation). This 'c'

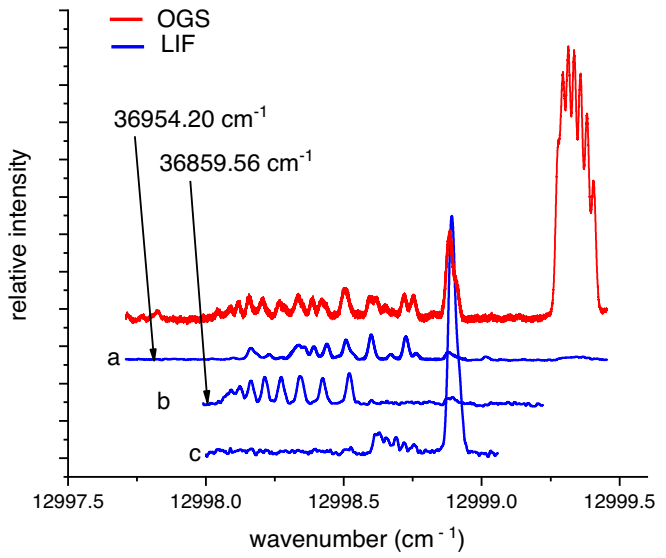

Fig. 4. Comparison of the optogalvanic (OGS) and laser induced fluorescence (LIF) spectra with different fluorescence lines as indicated at the left side of the LIF curves. The selected fluorescence lines are marked in Fig. 3 with letters 'fl (a)', 'fl(b)' and 'fl(c)' OGS spectrum is the same as in Fig. 1. The corresponding transitions are. For both examined lines, a and b, the respective upper new level is indicated with an arrow.
a: 23955.68 cm^{-1}, $J = 13/2$ to 36,954.20 cm^{-1}, $J = 13/2$,
b: 23861.17 cm^{-1}, $J = 9/2$ to 36,859.56 cm^{-1}, $J = 11/2$,
c: 24357.92 cm^{-1}, $J = 15/2$ to 37,356.81 cm^{-1}, $J = 17/2$ (this line was not analyzed further in this study and is not listed in Table 2).

line in Fig. 4 was classified as a transition to already known levels and is not discussed further in this paper. Nevertheless, the curve is shown here to demonstrate the complexity and density of the spectrum.

The wavelength of the fluorescence lines should actually help to identify one of the two levels of the laser transition and thus facilitate the search for the unknown level. This was possible in about half of the cases. Negative fluorescence in particular is very helpful, as in all but one case the lower level is the known level. In all the cases presented here, the upper level was unknown. Therefore, it was more difficult to identify the new level when only positive fluorescence lines appeared in the monochromator scan. In cases where the fluorescence wavelengths fail to provide a definitive conclusion, the hfs fingerprint can be used to identify the levels. In this study, all new levels were successfully identified using the fingerprints. The positive fluorescence lines were then used to confirm the existence of the new levels.

However, due to collision-induced effects in the hollow cathode plasma, it often happens that lines in the monochromator scans also appear as laser-induced fluorescence, although neither of the two levels is involved in the laser transition. For this reason, there were sometimes still doubts about the new levels at this point.

If a potential new level was predicted based on the wavelength of the fluorescence lines and/or the hfs fingerprint, further transitions to this level were searched for to obtain final confirmation. Corresponding transitions were searched for using both the laser and the FT spectrum.

The hfs analysis allows a clear determination of the J quantum number for all new levels.

5. Results

The results of the laser measurements are summarized in Tables 2, 3 and 4.

A list of all investigated LIF lines, sorted by wavelength, is given in Table 2. The wavenumbers, σ, are the center-of-gravity (cg) of the hfs resulting from the fit of the hfs. The given values are the mean values of all the measurements taken for each line. The cg wavenumbers were determined relative to the starting wavenumber measured with the wavemeter as described in Section 2 to an absolute accuracy of 200 MHz or 0.007 cm^{-1}. The cg wavelength in the air λ_{air} is calculated from the cg wavenumber according to [32].

Since the spectral accuracy of the calibrated spectra [18–22] is within 0.005 cm^{-1}, which is slightly better than the accuracy of the wavemeter, the energy level values for the new levels were determined from the FT lines, as briefly described in the following section. The energy level values for the new levels given in Tables 2, 3 and 4 are the results of the analysis of the FT spectra presented in Table 5. The fourth column of Table 2 lists the difference $\Delta\sigma$ between the energy levels and the experimental wavenumber. The difference in $\Delta\sigma$ is for most of the lines significantly higher than the accuracy of the wavemeter. The same behavior is observed for FT lines and is due to large inaccuracies in the energy values of the known levels.

The value in the third column shows the signal-to-noise ratio (SNR) in the Ho—Ar FT spectra of unclassified spectral lines given in [21,22].

As mentioned in the introduction, four of the levels we discovered were also discovered and first published by the research group at the Poznan University of Technology (Poland) [12,14]. For the sake of completeness, the lines corresponding to these four levels are also marked with an asterisk in Table 2.

A list of all new levels together with their hfs data is given in Table 3. The line data used in Table 2 to measure the levels are repeated here for the sake of clarity. The hfs constants A and B of the new levels are given as the results of individual lines and - if more than one line was measured - as weighted mean values.

The values and their uncertainties are calculated using the same method as given in [11].

As mentioned above, all LIF spectra were recorded and fitted five or more times. The constants A_{exp} and B_{exp} in Table 3 are the mean values of the fit results of all corresponding measurements. The uncertainties given in brackets are calculated using the following formula:

$$\Delta A_{exp} = \sqrt{(\Delta A_{Fitter})^2 + (\Delta s_A)^2 + (\Delta A_{fixed})^2}\,, \quad (1)$$

where ΔA_{Fitter} is the standard deviation of A resulting from the hfs fit, Δs_A is the standard deviation corresponding to the mean value of the different measurements and ΔA_{fixed} is the uncertainty of the fixed A value, as given in Table 1. If all hfs constants have been freely adjusted in the fit, the contribution from ΔA_{fixed} is omitted. A similar formula applies to the B constants.

In cases, when the hfs constants A_{exp} and B_{exp} of a level had been measured with several lines, the weighted mean values A_{mean} and B_{mean} were calculated. The square of the reciprocal of the uncertainties ΔA_{exp} and ΔB_{exp}, respectively, were used as weights. The uncertainties of the individual values and the dispersion of the various values have been taken into account in the calculation of the corresponding uncertainties. For energy levels, measured with only one line, the uncertainties may be underestimated. This is because the uncertainties only account for statistical uncertainty, and not systematic deviations caused for example by couplings during the fit. These deviations only become apparent when comparing the results for several lines. As a result, the stated uncertainties may not accurately reflect the real values, which could potentially be greater.

A_{exp} and B_{exp} for the already known levels, which are a by-product of this investigation of new levels, are listed in Table 4. This table is structured in the same way as Table 3, except that the last three columns contain literature values for comparison, if available.

For most levels with already known hfs constants, our new values within the error bars agree with the values from the references.

Table 2
List of Ho I lines measured with LIF spectroscopy to identify new levels, with classification (new levels are emphasized in bold font).

line					lower level				upper level			
λ_{air} (nm)	σ (cm^{-1})		SNR	$\Delta\sigma$ (cm^{-1})	E (cm^{-1})		J	p	E (cm^{-1})		J	p
698.742	14,307.48	*	13	−0.03	24,357.92	f	15/2	o	38,665.37		13/2	e
712.356	14,034.05		9	−0.03	24,014.22	f	13/2	e	**38,048.24**		11/2	o
713.943	14,002.85		4	0.02	17,059.35	f	13/2	e	**31,062.22**		11/2	o
714.437	13,993.18	*	3	0.07	24,263.96		17/2	e	38,257.19		19/2	o
719.416	13,896.34	*	22	0.06	24,360.81		17/2	e	38,257.19		19/2	o
721.864	13,849.21	*	4	−0.02	23,885.74		17/2	o	37,734.93		19/2	e
722.232	13,842.15		4	0.09	18,821.25		11/2	e	**32,663.47**		11/2	o
726.429	13,762.17		3	−0.07	24,014.22	f	13/2	e	**37,776.32**		13/2	o
741.982	13,473.71		18	0.01	18,491.21		11/2	e	**31,964.93**		13/2	o
744.565	13,426.96		8	0.02	24,660.80	f	15/2	e	**38,087.78**		15/2	o
745.148	13,416.45	*	5	−0.04	24,660.80	f	15/2	e	38,077.21		13/2	o
750.129	13,327.37		–	−0.05	29,443.09		17/2	o	**42,770.41**		15/2	e
750.912	13,313.47		20	−0.07	18,651.53	f	15/2	e	**31,964.93**		13/2	o
755.128	13,239.15		–	0.01	29,531.25	f	17/2	o	**42,770.41**		15/2	e
756.912	13,207.93		14	0.08	26,957.70	f	15/2	e	**40,165.71**		13/2	o
760.614	13,143.66		48	0.02	18,821.25		11/2	e	**31,964.93**		13/2	o
761.405	13,130.00		–	0.02	26,947.33		13/2	e	**40,077.35**	f	11/2	o
762.757	13,106.73		44	0.01	18,858.19		13/2	e	**31,964.93**		13/2	o
766.909	13,035.77		–	0.03	24,740.52	f	13/2	e	**37,776.32**		13/2	o
767.005	13,034.14		–	0.06	24,740.52	f	13/2	e	**37,774.72**		11/2	o
767.574	13,024.48		7	−0.05	27,141.28		13/2	e	**40,165.71**		13/2	o
769.108	12,998.50		–	0.02	23,955.68	f	13/2	e	**36,954.20**		13/2	o
769.119	12,998.32		–	0.07	23,861.17	f	9/2	e	**36,859.56**		11/2	o
771.141	12,964.23		–	0.08	29,443.09	f	17/2	o	**42,407.4**		17/2	e
771.151	12,964.07		19	0.00	**27,113.28**		11/2	e	**40,077.35**		11/2	o
772.815	12,936.16		4	−0.09	27,141.28		13/2	e	**40,077.35**		11/2	o
774.177	12,913.39		5	0.01	23,946.16	f	11/2	e	**36,859.56**		11/2	o
775.295	12,894.77		–	−0.06	29,443.09		17/2	o	**42,337.80**		17/2	e
780.636	12,806.54		–	0.01	29,531.25		17/2	o	**42,337.80**		17/2	e
785.269	12,730.98		–	0.06	26,922.40		15/2	o	**39,653.44**		13/2	e
786.282	12,714.58		–	0.15	29,692.67	f	19/2	o	**42,407.4**		17/2	e
798.468	12,520.54		–	−0.09	27,556.90	f	9/2	e	**40,077.35**		11/2	o
799.540	12,503.75		–	0.00	29,834.05	f	15/2	o	**42,337.80**		17/2	e
803.824	12,437.11		–	0.03	27,640.21	f	11/2	e	**40,077.35**		11/2	o
832.836	12,003.87		–	0.06	27,649.51		15/2	o	**39,653.44**		13/2	e

Notes: *: no new level involved in this line (only level discovered by us but already published in [12,14]); SNR: if, line is also observed in the FT spectra, signal-to-noise ratio (SNR) from Ho—Ar FT spectrum [21,22] is given; lines without SNR value are not observed in the FT spectra; $\Delta\sigma = E_{upper} - E_{lower} - \sigma$: difference between the difference of the level energies and the experimental wavenumber; f: hfs constants A and B of this level fixed during fitting process.

6. Investigation of FT lines

As mentioned above, available FT spectra were analyzed with regard to the new levels. For the entire wavelength range of the FT spectra, which covers the UV range from 317 nm to 400 nm [18,19], the VIS range from 400 nm to 700 nm [20,21] and the NIR range from 700 nm to 1750 nm [22], all theoretically possible transitions to all known energy levels were calculated and checked to see whether a signal was visible at the corresponding wavelength. For this purpose, the program Elements [30,31] was used.

Table 5 lists all FT lines that can be classified as transitions to new levels, sorted by new level and wavelength. The observed cg wavelength was read from the FT spectra by comparing a simulated hfs with the corresponding section of the FT spectrum. The program Elements allows the two spectra to be shifted along the wavelength axis until a perfect overlap is achieved. This makes it possible to determine the cg quite accurately. For lines with SNR higher than 10, the reading accuracy is estimated to be better than 0.0001 nm, and for lines with SNR smaller or equal to 10 to be better than 0.0005 nm. These values were converted into wavenumbers (for the corresponding wavelengths) and the value of 0.005 cm^{-1} for the calibration accuracy was added. The resulting values are listed as u_σ in the third column of Table 5. In the sixth column, $\Delta\sigma$, the difference between the energy levels and the observed wavenumber is given.

The energy values given for the new values are the weighted means of the energy levels, calculated according to the Ritz principle for each line as the sum of the wavenumber and the energy level of the lower level. The standard deviation Δs, which corresponds to the mean values of E, is higher than the uncertainties of the wavenumbers u_σ for some levels, e.g. for the level 40,077.35 cm^{-1}, where the highest value of u_σ is 0.04 cm^{-1} and the standard deviation is 0.09 cm^{-1}. This is due to the large inaccuracies of the energy level values for Ho I.

The same information, for levels already published by [12,14] and also discovered in this work is given in Table 6.

7. Comparison with results from semi-empirical calculations

In [26,34] a semi-empirical investigation of fine and hyperfine structure investigations of Ho I are presented for levels of even and odd parity. We compared our new levels with the list of calculated energies given in these publications. The lowest new level could be clearly assigned. We have also selected an assignment for another four low-lying levels, although in all cases one of the values for Energy E or hfs constants A or B does not match so well. These levels are compiled in Table 7.

For the lowest new level, the agreement for energy, as well as for A and B is excellent, demonstrating the high quality of the theoretical predictions given by the semi-empirical calculations. This is the only new level with even parity lying below 39,000 cm^{-1}. All of the higher energy levels are difficult to assign since the levels are close together and

Table 3
New levels together with their hyperfine structure constants A and B (in MHz). Energy values and error bars resulting from the analysis of FT lines (see Table 5).

E (cm^{-1})	J	p	λ_{air} (nm)	A_{exp}	B_{exp}	A_{mean}	B_{mean}
27,113.28 (0.02)	11/2	e	771.151 f	1174.0 (1.3)†	−2127 (16)†		
31,062.22 (0.02)	11/2	o	713.943 f	1195.5 (0.9)†	653 (48)†		
31,964.93 (0.03)	13/2	o	760.614	594.8 (0.6)	−834 (36)	594.4 (0.5)	−849 (28)
			750.912 f	594.1 (0.6)	−883 (33)		
			741.982	593.6 (2.3)	−729 (80)		
			762.757	595.0 (2.1)	−847 (59)		
32,663.47 (0.04)	11/2	o	722.232	915.0 (2.0)†	−77 (35)†		
36,859.56 (0.03)	11/2	o	769.119 f	540 (5)	718 (310)	538 (4)	600 (120)
			774.177 f	535 (5)	580 (130)		
36,954.20 (0.04)	13/2	o	769.108 f	1205.8 (1.0)†	1107 (21)†		
37,774.72 (0.05)	11/2	o	767.005 f	1255.9 (1.2)†	1541 (54)†		
37,776.32 (0.04)	13/2	o	726.429 f	1082.8 (0.8)	−2098 (46)	1083.6 (1.1)	−2070 (56)
			766.909 f	1086.0 (1.5)	−1848 (130)		
38,048.24 (0.03)	11/2	o	712.356 f	666.1 (0.3)†	−387 (110)†		
38,087.78 (0.06)	15/2	o	744.565 f	1015.3 (0.7)†	−540 (33)†		
39,653.44 (0.04)	13/2	e	785.269	766.5 (0.4)	590 (26)	767.0 (0.6)	575 (16)
			832.836	768.4 (0.7)	567 (18)		
40,077.35 (0.08)	11/2	o	798.468 f	1143.9 (0.6)	−645 (21)	1143.8 (0.5)	−635 (10)
			761.405	1144.6 (2.0)	−640 (12)		
			772.815	1146 (3)	−642 (19)		
			771.151	1142.8 (0.8)	−602 (24)		
			803.824 f	1145.3 (1.6)	−621 (31)		
40,165.71 (0.07)	13/2	o	756.912	1870.8 (1.3)	−1129 (81)	1869.9 (0.7)	−1043 (13)
			767.574	1869.6 (0.8)	−1041 (13)		
42,337.80 (0.07)	17/2	e	780.636	1405.1 (2.5)	−298 (100)		
			775.295	1409.6 (0.7)	−155 (56)	1409.6 (0.8)	−178 (52)
			799.540 f	1413.3 (1.9)	−136 (110)		
42,407.4 (0.1)	17/2	e	771.141 f	980 (3)	−681 (150)	980.0 (2.1)	−655 (110)
			786.282 f	980 (3)	−627 (150)		
42,770.41 (0.04)	15/2	e	755.128 f	1289 (3)	943 (190)	1284.8 (0.6)	945 (39)
			750.129	1284.7 (0.5)	945 (40)		

Notes: f: hfs constants A and B of the other level were fixed during fitting process.
† Uncertainty calculated from only one line.

Table 4
Experimental hyperfine structure constants A and B (in MHz) for already known levels, together with values from literature if available.

E (cm^{-1})	J	p	λ_{air} (nm)	A_{exp}	B_{exp}	A_{mean}	B_{mean}	A_{ref}	B_{ref}	ref.
18,491.21	11/2	e	741.982	836.7 (2.5)†	−244 (97)†			842 (2)	−380 (29)	[25]
18,821.25	11/2	e	722.232	265.2 (1.0)	−417 (58)	265.0 (0.7)	−413 (31)	264.7 (0.6)	−446 (33)	[9]
18,821.25	11/2	e	760.614	264.9 (1.0)	−411 (37)					
18,858.19	13/2	e	762.757	466 (3)†	−3117 (59)†			465.45 (23)	−3158 (14)	[11]
23,885.74	17/2	o	721.864	705.8 (0.8)†	−1697 (34)†			708.9 (1.5)	−1473 (95)	[26]
24,263.96	17/2	e	714.437	716.7 (1.4)†	1058 (100)†					tw
24,360.81	17/2	e	719.416	658 (3)†	−584 (330)†					tw
26,922.40	15/2	o	785.269	1115.1 (0.6)†	−891 (26)†			1118 (3)	−908 (15)	[2]
26,947.33	13/2	e	761.405	582.1 (0.6)†	−162 (47)†					tw
27,141.28	13/2	e	767.574	1446.3 (0.4)	−1742 (11)	1446.3 (0.4)	−1752 (16)	1444.4 (1.9)	−1820 (100)	[23]
27,141.28	13/2	e	772.815	1450 (4)	−1817 (27)					
27,649.51	15/2	o	832.836	993.1 (0.5)†	1600 (28)†			991.6 (1.4)	1578 (88)	[33]
29,443.09	17/2	o	750.129	1055.5 (0.5)	2242 (39)	1055.7 (0.4)	2251 (36)	1061 (3)	2084 (150)	[2]
29,443.09	17/2	o	775.295	1055.9 (0.6)	2281 (72)					
29,531.25	17/2	o	780.636	1210.4 (2.5)†	−19 (110)†			1218.2 (3.0)	122 (18)	[10]
37,734.93 *	19/2	e	721.864	769.2 (0.7)†	402 (29)†			769.3 (0.1)	555 (88)	[14]
38,077.21 *	13/2	o	745.148 f	1408.3 (0.6)†	−211 (57)†			1408.9 (1.7)	−239 (35)	[12]
38,257.19 *	19/2	o	714.437	118.6 (1.3)	−1354 (140)	120.0 (1.0)	−1340 (87)	118.0 (1.6)	−1400 (121)	[12]
		o	719.416	120.9 (1.1)	−1332 (110)					
38,665.37 *	13/2	e	698.742 f	895.2 (1.1)†	−691 (140)†			901.6 (1.8)	−781 (218)	[12]

Notes: Values from [2] are converted from 10^{-3} cm^{-1} to MHz; f: hfs constants A and B of the other level were fixed during fitting process; tw: this work.
†: Uncertainty calculated from only one line.

sometimes have similar A and B values.

For the odd-parity levels, we have assigned our new levels up to 36,900 cm^{-1}. The assignment of the higher levels should be carried out as part of a recalculation of the semi-empirical analysis of the configuration systems for even and odd parity.

8. Conclusions and outlook

With this work, we have made a further contribution to the determination of laboratory data of complex atoms. Altogether 20 energy levels have been discovered – however, four of them were also found by other researchers and published more quickly. Additionally, for three already known levels new hfs data are provided.

Table 5
List of Holmium lines from the FT spectrum [19,21,22], classified by the new levels.

						other level	
λ_{air} (nm)	σ (cm^{-1})	u_σ (cm^{-1})	SNR	com.	$\Delta\sigma$ (cm^{-1})	E (cm^{-1})	J
27113.28(0.02) cm^{-1}, $J = 11/2$, e							
460.8371	21,693.567	0.029	8		0.013	5419.70	13/2
540.1529	18,508.130	0.022	9		−0.010	8605.16	11/2
771.1504	12,964.071	0.007	19	LIF	−0.001	40,077.35	11/2
31062.22(0.02) cm^{-1}, $J = 11/2$, o							
456.1776	21,915.145	0.010	40		−0.005	9147.08	13/2
534.1058	18,717.677	0.023	8	b	−0.007	12,344.55	13/2
713.9434	14,002.852	0.015	4	LIF	0.018	17,059.35	13/2
31964.93(0.03) cm^{-1}, $J = 13/2$, o							
438.1304	22,817.845	0.031	8		0.005	9147.08	13/2
509.3887	19,625.904	0.024	6	b	−0.014	12,339.04	15/2
662.8311	15,082.634	0.007	215		0.016	16,882.28	15/2
670.7054	14,905.562	0.007	19		0.018	17,059.35	13/2
741.9820	13,473.706	0.007	18	LIF	0.014	18,491.21	11/2
750.9126	13,313.464	0.007	20	LIF	−0.064	18,651.53	15/2
760.6131	13,143.670	0.007	48	LIF	0.010	18,821.25	11/2
762.7555	13,106.753	0.007	44	b, LIF	−0.013	18,858.19	13/2
32663.47(0.04) cm^{-1}, $J = 11/2$, o							
492.0147	20,318.924	0.009	33		−0.004	12,344.55	13/2
722.2317	13,842.157	0.034	4	r LIF	0.063	18,821.25	11/2
1076.8080	9284.163	0.009	5		−0.004	23,379.31	11/2
36859.56(0.03) cm^{-1}, $J = 11/2$, o							
546.4550	18,294.686	0.022	8	b	−0.026	18,564.90	13/2
610.8485	16,366.141	0.018	5	d	0.019	20,493.40	11/2
774.1774	12,913.383	0.013	5	LIF	0.017	23,946.16	11/2
36954.20(0.04) cm^{-1}, $J = 13/2$, o							
406.1388	24,615.171	0.011	14	b	−0.011	12,339.04	15/2
406.2302	24,609.637	0.035	7		0.013	12,344.55	13/2
472.4111	21,162.083	0.029	17	r	−0.013	15,792.13	11/2
499.4432	20,016.714	0.025	7		0.056	16,937.43	11/2
549.3576	18,198.022	0.022	6	b	−0.042	18,756.22	15/2
37774.72(0.05) cm^{-1}, $J = 11/2$, o							
349.2130	28,627.627	0.013	20		0.013	9147.08	13/2
404.8790	24,691.760	0.011	27		0.030	13,082.93	11/2
570.1799	17,533.460	0.020	7		−0.050	20,241.31	13/2
37776.32(0.04) cm^{-1}, $J = 13/2$, o							
404.8518	24,693.420	0.011	12		−0.030	13,082.93	11/2
726.4331	13,762.100	0.014	3	LIF	0.000	24,014.22	13/2
38048.24(0.03) cm^{-1}, $J = 11/2$, o							
388.9386	25,703.715	0.038	6		−0.025	12,344.55	13/2
476.3102	20,988.852	0.009	158		0.038	17,059.35	13/2
520.9587	19,190.037	0.023	8		0.013	18,858.19	13/2
712.3574	14,034.029	0.015	9	LIF	−0.009	24,014.22	13/2
38087.78(0.06) cm^{-1}, $J = 15/2$, o							
345.4361	28,940.619	0.047	8		0.081	9147.08	13/2
449.6654	22,232.519	0.010	41		−0.019	15,855.28	15/2
455.7947	21,933.556	0.010	13		0.014	16,154.21	15/2
467.6386	21,378.049	0.010	20		−0.089	16,709.82	17/2
506.1877	19,750.012	0.025	10		−0.032	18,337.80	17/2
744.5654	13,426.955	0.014	8	LIF	0.025	24,660.80	15/2
39653.44(0.04) cm^{-1}, $J = 13/2$, e							
480.9616	20,785.870	0.009	23		0.030	18,867.54	13/2
490.6233	20,376.546	0.009	13	b	−0.026	19,276.92	15/2
40077.35(0.08) cm^{-1}, $J = 11/2$, o							
370.3421	26,994.378	0.041	6		0.042	13,082.93	11/2

(*continued on next page*)

Table 5 (*continued*)

						other level	
λ_{air} (nm)	σ (cm^{-1})	u_σ (cm^{-1})	SNR	com.	$\Delta\sigma$ (cm^{-1})	E (cm^{-1})	J
655.6906	15,246.884	0.017	4		0.036	24,830.43	11/2
683.6290	14,623.783	0.007	12	b, a	0.077	25,453.49	9/2
689.1664	14,506.281	0.016	10		−0.081	25,571.15	13/2
772.8142	12,936.161	0.013	4	LIF	−0.091	27,141.28	13/2
40165.71 (0.07) cm^{-1}, $J = 13/2$, o							
681.8315	14,662.333	0.016	8	b	0.047	25,503.33	11/2
684.9956	14,594.607	0.016	10	b	−0.047	25,571.15	13/2
756.9120	13,207.938	0.007	14	LIF	0.072	26,957.70	15/2
767.5731	13,024.491	0.013	7	LIF	−0.061	27,141.28	13/2
42337.80 (0.07) cm^{-1}, $J = 17/2$, e							
548.5214	18,225.767	0.022	10	b	−0.007	24,112.04	15/2
548.6177	18,222.568	0.022	10		0.062	24,115.17	17/2
566.1096	17,659.522	0.008	11		0.028	24,678.25	19/2
672.4173	14,867.613	0.016	7		−0.083	27,470.27	19/2
42407.4 (0.1) cm^{-1}, $J = 17/2$, e							
448.6439	22,283.139	0.030	4		−0.009	20,124.27	19/2
42770.41 (0.04) cm^{-1}, $J = 15/2$, e							
535.8020	18,658.422	0.022	10		−0.052	24,112.04	15/2
535.8940	18,655.217	0.022	8		0.023	24,115.17	17/2
550.0339	18,175.650	0.008	18		0.010	24,594.75	13/2
664.4437	15,046.028	0.016	5		0.022	27,724.36	13/2

Notes: λ_{air}: observed center-of-gravity wavelength in air from FT spectrum; σ: observed center-of-gravity vacuum wavenumber of the transition; SNR: observed signal-to-noise ratio of the transition in the Ho-Ar-spectrum; u_σ: uncertainty in observed wavenumber from FT spectra; $\Delta\sigma = E_{upper} - E_{lower} - \sigma$: difference between the difference of the level energies and the observed wavenumber; comment (com.): a: hfs constants A and B of lower level unknown; b: blend not disturbing the determination of cg; r: blend which reduces the accuracy in the determination of cg; LIF: also measured with LIF.

Table 6
List of Holmium lines from the FT spectrum [19,21,22], classified by the levels already published in [12,14], but also discovered by us.

						other level	
λ_{air} (nm)	σ (cm^{-1})	u_σ (cm^{-1})	SNR	com.	$\Delta\sigma$ (cm^{-1})	E (cm^{-1})	J
37734.93 (0.02) cm^{-1}, $J = 19/2$, e							
573.9246	17,419.059	0.008	118		−0.019	20,315.89	17/2
583.9116	17,121.133	0.008	84		−0.003	20,613.80	17/2
688.3386	14,523.727	0.007	14		−0.007	23,211.21	19/2
721.8656	13,849.178	0.015	4	LIF	0.012	23,885.74	17/2
38077.21 (0.04) cm^{-1}, $J = 13/2$, o							
471.6797	21,194.900	0.027	8	b	0.030	16,882.28	15/2
475.6536	21,017.826	0.009	25	b	0.034	17,059.35	13/2
514.6378	19,425.731	0.009	14	b	−0.051	18,651.53	15/2
710.8895	14,063.007	0.015	4	b	−0.017	24,014.22	13/2
745.1499	13,416.423	0.014	5	b, LIF	−0.013	24,660.80	15/2
38257.19 (0.05) cm^{-1}, $J = 19/2$, o							
458.1845	21,819.153	0.040	14	r	0.027	16,438.03	17/2
463.9624	21,547.439	0.010	62	b	−0.049	16,709.82	17/2
501.8829	19,919.412	0.009	93		−0.002	18,337.80	17/2
714.4373	13,993.172	0.035	3	r, LIF	−0.029	24,263.96	17/2
719.4157	13,896.340	0.007	22	LIF	0.060	24,360.81	17/2
38665.37 (0.08) cm^{-1}, $J = 13/2$, e							
515.6245	19,388.557	0.009	14	b	−0.107	19,276.92	15/2
537.3540	18,604.534	0.008	30	b	0.076	20,060.76	11/2
550.1577	18,171.558	0.008	22		0.052	20,493.76	13/2
698.7426	14,307.475	0.007	13	LIF	−0.025	24,357.92	15/2

Based on our new data together with the data from other publications from the last few years, it would be recommended to perform again a semi-empirical calculation of the fine structure and hyperfine structure of Ho I for even and odd parity.

The large inaccuracies of the level energy values for Ho I are noticeable in this work, as already observed in previous works [18,20,22]. This fact prevents a more accurate determination of the energy values for the newly discovered levels. A revision of all Ho I

Table 7
Comparison of calculated level energies and hfs constants A and B from [26,34] with our new experimental data; term and corresponding percentage in the last two columns according to [26,34].

E_{calc}	E_{exp}	ΔE	A_{calc}	A_{exp}	ΔA	B_{calc}	B_{exp}	ΔB	Term	perc.
even parity, $J = 11/2$										
27,176	27,113.28	63	1147	1174.0	−27	−2365	−2127	−238	$4f^{11}$ (^{4}I)6s6p $^6I_{11/2}$	34.9%
odd parity, $J = 11/2$										
30,966	31,062.22	−66	1144	1195.5	−51	−1160	653	1813	$4f^{11}$ (^{4}I)5d6s $^4H_{11/2}$	16.4%
32,687	32,663.49	34	1037	915.0	122	172	−77	249	$4f^{10}$ (^{5}I)5d6s6p $^8F_{11/2}$	13.6%
36,753	36,859.56	−107	686	538	148	615	600	15	$4f^{10}$ (^{5}I)5d6s6p $^8L_{11/2}$	13.6%
odd parity, $J = 13/2$										
31,878	31,964.93	−86	703	594.4	109	−446	−849	403	$4f^{10}$ (^{5}I)5d6s6p $^8G_{13/2}$	7.2%

energy levels is planned by our research group for the future and is already in progress.

CRediT authorship contribution statement

Seda Kın Barka: Writing – original draft, Investigation, Formal analysis. **Günay Başar:** Writing – review & editing, Investigation, Conceptualization. **Sophie Kröger:** Writing – original draft, Investigation, Formal analysis, Conceptualization. **Gönül Başar:** Writing – review & editing, Investigation, Formal analysis, Conceptualization.

Declaration of competing interest

The authors declare that they have no known competing financial interests or personal relationships that could have appeared to influence the work reported in this paper.

Data availability

Data will be made available on request.

Acknowledgement

This work was supported by the Istanbul University Scientific Research Project No. 39701.

We would like to acknowledge Prof. Ruvin Ferber and his team at the Laser Center of the University of Latvia in Riga for their good cooperation and the opportunity to measure the FT spectra in their laboratory.

References

[1] N.J. Stone, Table of nuclear magnetic dipole and electric quadrupole moments, At. Data Nucl. Data Tables 90 (2005) 75, https://doi.org/10.1016/j.adt.2005.04.001.
[2] J.F. Wyart, P. Camus, J. Vergès, Etude du spectre de l'holmium atomique: I. Spectre d'émission infrarouge niveaux d'énergie de Ho I et structures hyperfines, Physica B +C 92 (1977) 377, https://doi.org/10.1016/0378-4363(77)90137-1.
[3] W.C. Martin, R. Zalubas, L. Hagan, Atomic Energy Levels–The Rare Earth Elements, Institute for Basic Standards, National Bureau of Standards, Washington, D.C 1, 2023, p. 1978.
[4] S. Kröger, J.F. Wyart, P. Luc, Theoretical interpretation of hyperfine structures in doubly-excited configurations $4f^{10}5d6s6p$ and $4f^{10}5d^26s$ and new energy levels in neutral holmium (ho I), Phys. Scr. 55 (1997) 579, https://doi.org/10.1088/0031-8949/55/5/010.
[5] A. Kramida, Y. Ralchenko, J. Reader, NIST ASD Team, NIST Atomic Spectra Database (ver. 5.11), [Online], Available, https://physics.nist.gov/asd [2024, January 16]. National Institute of Standards and Technology, Gaithersburg, MD, 2024, https://doi.org/10.18434/T4W30F.
[6] W.J. Childs, D.R. Cok, L.S. Goodman, New line classifications in ho I based on high-precision hyperfine-structure measurement of low levels, J. Opt. Soc. Am. 73 (1983) 151, https://doi.org/10.1364/JOSA.73.000151.
[7] E.A. Den Hartog, L.M. Wiese, J.E. Lawler, Radiative lifetimes of ho I and ho II, J. Opt. Soc. Am. B 16 (1999) 2278, https://doi.org/10.1364/JOSAB.16.002278.
[8] Yu.M. Smirnov, Excitation of low-lying even levels of the holmium atom in the electron-atom collisions, Opt. Spectrosc. 114 (2013) 485, https://doi.org/10.1134/S0030400X13040188.
[9] B. Furmann, D. Stefanska, M. Suski, S. Wilman, Identification of new electronic levels in the holmium atom and investigation of their hyperfine structure, JQSRT 219 (2018) 117, doi:10.1016/j.jqsrt.2018.08.005.
[10] B. Furmann, D. Stefanska, S. Wilman, M. Chomski, M. Suski, Hyperfine structure studies of the odd-parity electronic levels in the holmium atom. II: New levels, JQSRT 235 (2019) 70, https://doi.org/10.1016/j.jqsrt.2019.06.005.
[11] G. Başar, G. Başar, B. Özdalgıç, et al., Laser spectroscopic investigation of atomic holmium in the wavelength range from 780 nm to 830 nm: Hyperfine structure measurements and a new energy level, JQSRT 243 (2020) 106809, https://doi.org/10.1016/j.jqsrt.2019.106809.
[12] M. Chomski, B. Furmann, M. Suski, et al., Determination of the energies of new electronic levels of the holmium atom and investigation of their hyperfine structure, JQSRT 297 (2023) 108480, https://doi.org/10.1016/j.jqsrt.2022.108480.
[13] D. Bingöl, G. Başar, G. Başar, et al., Verification of the Existence of Recently Published New Energy Levels of Atomic Holmium, Physics and Astronomy Reports 1 (2023) 85, https://doi.org/10.26650/PAR.2023.00010.
[14] B. Furmann, M. Klemska, S. Mieloch, D. StefaÅska, Hyperfine structure and even-parity new levels evaluation in the holmium atom, JQSRT 316 (2024) 108903, https://doi.org/10.1016/j.jqsrt.2024.108903.
[15] I.K. Öztürk, G. Başar, A. Er, F. Güzelçimen, G. Başar, S. Kröger, New energy levels of atomic niobium by laser induced fluorescence spectroscopy in the near infrared, J. Phys. B Atomic Mol. Phys. 48 (2015) 015005, https://doi.org/10.1088/0953-4075/48/1/015005.
[16] I.K. Öztürk, G. Başar, G. Başar, et al., New energy levels of atomic lanthanum with small total angular momentum quantum number discovered by laser spectroscopic methods in the near IR, JQSRT 253 (2020) 107100, https://doi.org/10.1016/j.jqsrt.2020.107100.
[17] D. Messnarz, G.H. Guthöhrlein, Investigation of the hyperfine structure of ta I-lines (IV), Eur. Phys. J. D 12 (2000) 269, https://doi.org/10.1007/s100530070022.
[18] N. Al-Labady, B. Özdalgç, A. Er, et al., Line Identification of Atomic and Ionic Spectra of Holmium in the Near-UV. Part I. Spectrum of Ho I, APJS 228 (2017) 16, https://doi.org/10.3847/1538-4365/228/2/16.
[19] G. Başar, F. Güzelçimen, B. Özdalgç, et al., Line Identification of Atomic and Ionic Spectra of Holmium in the Near-UV. II. Spectra of Ho II and Ho III, APJS 228 (2017) 17, https://doi.org/10.3847/1538-4365/228/2/17.
[20] B. Özdalgç, F. Güzelçimen, I.K. Öztürk, et al., Line identification of atomic and ionic spectra of holmium in the visible spectral range. I. Spectrum of Ho I, APJS 240 (2019) 27, https://doi.org/10.3847/1538-4365/aaf9b2.
[21] B. Özdalgç, G. Başar, F. Güzelçimen, et al., Line Identification of Atomic and Ionic Spectra of Holmium in the Visible Spectral Range. II. Spectrum of Ho II and Ho III, APJS 240 (2019) 28, https://doi.org/10.3847/1538-4365/aaf9b5.
[22] M. Zengin, S.K. Barka, I.K. Öztürk, et al., Line Identification of Atomic and Ionic Spectra of Holmium in the Near Infrared Spectral Range From 700 nm to 1750 nm, 2024.
[23] B. Özdalgç, G. Başar, S. Kröger, Hyperfine Structure Analysis of Atomic Holmium in an FT Spectrum in the Visible Spectral Range, APJS 244 (2019) 41, https://doi.org/10.3847/1538-4365/ab4262.
[24] A. Zeiser, S. Kröger, L. Pooyan-Weis, L. Windholz, G. Guthöhrlein, New version of the program FITTER for fitting atomic hyperfine structure in optical spectra including the calculation of confidence intervals, JQSRT 290 (2000) 108294, https://doi.org/10.1016/j.jqsrt.2022.108294.
[25] D. Stefanska, B. Furmann, Hyperfine structure investigations for the odd-parity configuration system in atomic holmium, JQSRT 206 (2018) 286, https://doi.org/10.1016/j.jqsrt.2017.11.019.
[26] D. Stefanska, J. Ruczkowski, M. Elantkowska, B. Furmann, Fine- and hyperfine structure investigations of the even-parity configuration system of the atomic holmium, JQSRT 209 (2018) 180, https://doi.org/10.1016/j.jqsrt.2018.01.010.
[27] Ł.M. Sobolewski, L. Windholz, J. Kwela, R. Drozdowski, LIF spectra of magnetic splitting of lines of atomic vanadium, JQSRT 237 (2019) 106639, https://doi.org/10.1016/j.jqsrt.2019.106639.
[28] M. Faisal, L. Windholz, S. Kröger, Systematic investigations of the hyperfine structure constants of niobium I levels. Part I: Constants of upper odd parity energy levels between 16,672 and 31,025 cm^{-1} and discovery of a new level, JQSRT 245 (2020) 106873, https://doi.org/10.1016/j.jqsrt.2020.106873.
[29] L. Windholz, personal communication, 2020.
[30] L. Windholz, G.H. Guthöhrlein, Classification of Spectral Lines by Means of their Hyperfine Structure. Application to Ta I and Ta II Levels, Phys. Scr. T105 (2003) 55, https://doi.org/10.1238/Physica.Topical.105a00055.
[31] L. Windholz, personal communication, 2015.

[32] R. Peck, K. Reeder, Dispersion of air, J. Opt. Soc. Am. 62 (1972) 958, https://doi.org/10.1364/JOSA.62.000958.
[33] B. Furmann, D. Stefanska, M. Suski, S. Wilman, M. Chomski, Hyperfine structure studies of the odd-parity electronic levels of the holmium atom. I: Levels with known energies, JQSRT 24 (2019) 115, https://doi.org/10.1016/j.jqsrt.2019.05.028.
[34] M. Elantkowska, J. Ruczkowski, A. Sikorski, S. Wilman, Fine- and hyperfine structure investigations of the odd-parity configuration system in atomic holmium, JQSRT 237 (2019) 106642, https://doi.org/10.1016/j.jqsrt.2019.106642.